Semnan University

Journal of Heat and Mass Transfer Research

Journal homepage: https://jhmtr.semnan.ac.ir

ISSN: 2383-3068

Research Article

Stability of Magneto Double Diffusive Convection in Couple Stress Liquid with Chemical Reaction

Monal Bharty [a], Atul Kumar Srivastava [b]*, Hrishikesh Mahato [a]

[a] *Department of Mathematics, Central University of Jharkhand, Ranchi, 835222, India.*

[b] *Department of Mathematics, Sarala Birla University, Ranchi, 835103, India.*

ARTICLE INFO

Article history:

Received: 2023-03-22

Revised: 2023-11-01

Accepted: 2023-11-02

Keywords:

Chemical reaction;

Couple stress fluid;

External magnetic field;

Rayleigh number;

Stability analysis.

ABSTRACT

The effect of chemical reaction and external vertical magnetic field on the onset of the double diffusive convection in couple stress fluid between infinite horizontal parallel plates has been studied. The effectiveness of vertical magnetic field and chemical reaction were gauged by determining the values of Chandrashekhar number (Q) and Damköhler number (χ) in terms of other controlling parameters and shown their effect on stability of system through graphs. The entire investigation is performed in two parts: linear and weakly non-linear stability analysis. A comparative study is presented in stationary case of linear stability analysis for four types of bounding surfaces: (a) Realistic bounding surfaces i.e. Rigid-Rigid, Rigid-Free and Free-Rigid (R/R, R/F and F/R) (b) Non Realistic bounding surface i.e. Free-Free (F/F). However, oscillatory case and weakly non-linear stability analysis are restricted for Free-Free (F/F) boundary surfaces. Graphical representations are used to illustrate how different parameters affect stationary, oscillatory, finite-amplitude states and the amount of heat and mass transfer. By analysing the linear stability analysis, it is observed that the onset of convection is more dominant in oscillatory case than stationary. The stability criteria for Q came out as (in decreasing order) F/F>F/R>R/R>R/F which is different from the criteria came out for rest of the controlling parameters i.e F/R>R/R>F/F>R/F in stationary case. It is also reported that the Q, Couple stress parameter (C) and ratio of heat capacities on heat transfer γ is responsible for the delay of the onset of convection while χ (impact of chemical reaction) enhances the onset of convection. Non-linear stability analysis using the truncated representation of Fourier series method predicts the occurrence of sub-critical instability in the form of finite amplitude motion. The effect of Q, Lewis number Le, and solute Rayleigh number Ra_S, increased the amount of heat and mass transfer while C decreased. We also draw streamlines, isotherms, isohalines and magnetic streamlines for different time intervals (unsteady) i.e. for (0.01, 0.03, 0.009, 0.006) and showed the pattern of the onset of convection.

1. Introduction

In this study, we have investigated the role of chemical reaction and magnetic field in thermal convection of couple stress liquid in the absence of body couple. The majority of earlier research on thermal convection in couple stress fluid, which involves a variety of effects like rotation and chemical reactions, has been done in porous media using classical theory, which describes the polar effect in the presence of couple stress, body couple and non-symmetric tensors. The notion of couple stress fluids put forward by Stokes [1] is a fluid that has captured the interest of many researchers in fluid mechanics over the course of the last 50 years. The classical theory of Newtonian fluids is simply generalised into the

* **Corresponding author.**
E-mail address: atul.srivastava@sbu.ac.in

Cite this article as:
Bharty, M., Srivastava, A., Mahato, H., 2023. Stability of Magneto Double Diffusive Convection in Couple Stress Liquid with Chemical Reaction. *Journal of Heat and Mass Transfer Research*, 10(2), pp. 171 – 190.
https://doi.org/10.22075/JHMTR.2023.30246.1432

concept of couple stress fluids, which permits the sustenance of couple stresses and body couples in the fluid medium. The way the mechanical interactions in the fluid medium are described gives rise to the idea of couple stresses. Due to its importance in chemical engineering applications such as polymer-thickened oils, liquid crystals, polymeric suspensions [2], and physiological fluid mechanics [3], many researchers have looked into the couple stress fluid flow problems now a days.

The application of convection, mainly heat and mass transfer analysis, has a very significant role in daily life. The idea of natural convection flow has advanced significantly over the past few years and is now the fastest-growing study area. Out of many, some studies focused on natural convection between infinite fluid layers. Natural convection in a fluid layer, which was first studied by Bénard and Rayleigh in the early 20th century, is still a topic of ongoing research and offers a crucial paradigm for instability, extended pattern creation, and the change from a system into chaos or turbulence [4]. Despite substantial research being done on the Rayleigh-Bénard convection problem for Newtonian fluids, the thermal convection of non-Newtonian fluids has received comparatively little attention. Only a small number of researchers have explored Rayleigh-Bénard convection in fluids where the stress is not linearly proportional to the velocity gradient [5-7]. Using a vertical stretching surface, [8] examined the effects of some thermo-physical parameters on free convective heat and mass transfer at the lowest level of heat energy in the presence of suction. This analysis reveals that while temperature and concentration drop throughout the flow region, velocity increases as the value of the temperature-dependent fluid viscosity parameter rises. [9] evaluated the most recent research on wall-bounded flows of viscoelastic and viscoplastic non-Newtonian fluids, as well as instability and the subcritical transition to turbulence. In a horizontal channel with a couple-stress fluid sandwiched between two transparent viscous fluids, Umavathi et al. [10] investigated the steady laminar flow and heat transfer mathematically, demonstrating that the couple stress parameter has a promoting effect on the fluid's motion. Linear and non-linear double diffusive convection with the Soret effect in couple-stress liquids were examined analytically by [11]. Gupta et al. [12] studied the chaotic behaviour of thermal convection in a couple-stress liquid-saturated porous layer. In this work, it was discovered that there is a proportional relationship between the scaled couple stress parameter and the rescaled Rayleigh number. Also, analyzed that an increase in the level of couple stress parameter increases the level of chaos. A thermally radiative couple-stress magnetized liquid featuring Newtonian heating is examined by [13]. Misra et al. [14] have studied double diffusive electro-convection in a couple-stress anisotropic fluid-saturated rotating porous layer. In their research, they found that the electric field had a destabilising effect on thermodynamic convection, while the rotation couple stress parameter tended to stabilise the physical system under consideration. Transitions and bifurcations in couple-stress fluid saturated porous media using a thermal non-equilibrium model are investigated by [15]. By taking into account the couple-stress fluid on the porous layer, Yadav et al. [16] examined the impacts of temperature-dependent internal heat generation and the viscosity of thermal instability. Most of the above mentioned fluid flow problems dealt with single fluids. We are now presenting some new work with binary fluids, i.e., fluids with solutes. When temperature and dissolved substance both contribute to the fluid's buoyancy, this process is called thermosolutal convection. There are numerous industrial and geothermal applications that uses natural convection in binary fluids because of the simultaneous diffusion of temperature and solute. In some situations, changes in temperature, pressure, and the chemistry of the nearby rock have an impact on the solute concentration in the fluid [17]. The number of minerals dissolved in the fluid has an impact on the onset of convection. As a result, it becomes important to look into how chemical reactions affect the onset of convection. A variety of geological processes, such as the dolomitization of carbonate platforms [18], soil salinization [19], and heat transmission in geothermal reservoirs, may involve solutal and thermosolutal convection in porous media. The effects of reaction kinetics at a fluid interface or boundary have recently been taken into account for more complex chemical reaction flows. Interfacial reactions have been shown to prevent the elongation of a moving chemical front for longer durations of time, producing dispersion curves that are independent of time and finger growth rates that are lower than the initial growth rate of density-dependent instabilities in the absence of a reaction [20–21]. Srivastava et al. [22] described the impact of chemical reactions on the stability of thermosolutal convection of couple-stress fluid in a horizontal porous layer. In their paper, they elaborated on the applications of chemical reactions in detail and reported the effect of chemical reaction parameters on the stability of the system. The unsteady natural convection of coupled heat and mass transfer over a vertical plate immersed in a uniform porous medium with the impact of chemical

reactions and thermal radiation is numerically solved by [23]. According to the investigation, the Nusselt number rises with increases in thermal buoyancy, solutal buoyancy, Prandtl number, and Reynolds number; on the other hand, it falls with increases in permeability, inverse thermal radiation, chemical reaction, and Schmidt numbers. According to various theoretical and numerical studies, it is observed that thermal convection caused by an exothermic surface reaction on the bottom boundary, the Rayleigh number, is influenced by the Lewis number based on the reactant's diffusivity as well as the non-dimensional reaction rate. What would happen if we looked at the impact of an external magnetic field along with a chemical reaction and a binary couple-stress fluid? In the fields of planetary magnetosphere, aviation, and chemical engineering, magnetohydrodynamics (MHD) in free convection flows has significant applications. A number of research scholars have investigated the problem with MHD-free convection flows that involve heat and mass transport over different domains with different boundary conditions. The effect of a magnetic field on the onset of Bénard convection in variable-viscosity couple-stress fluids using the classical Lorenz model is studied by [24]. According to this study, the couple-stress parameter, the Chandrasekhar number, and the thermorheological parameter all have an impact on the onset of convection. On a convective MHD flow of a rotating fluid passing through a moving vertical isothermal plate under thermal radiation, chemical reaction, and heat source, [25] investigated the effects of radiation absorption and the Dufour effect. This study shows that as the Dufour number, radiation absorption, and heat source parameter increase, the fluid's velocity increases as well. Conversely, the parameters of the chemical reaction and rotation cause the velocity to slow down. The effects of slip conditions, wall characteristics, and heat transfer on MHD peristaltic transport of a Jeffrey fluid in a nonuniform porous channel have been explored by Saravana et al. [26]. Due to the instability mechanism known as magnetic buoyancy, a horizontal magnetic field that has become stratified with depth may become unstable. This instability plays a crucial role in the clumping of the interstellar medium, which encourages the formation of molecular clouds [27]. It is also one of the mechanisms responsible for the disruption of magnetic fields in accretion discs [28], and it is the leading candidate for the release of magnetic fields from the solar interior [29]. Narahari and Debnath [30] investigated the unsteady MHD-free convection flow through an accelerating vertical plate with continuous heat flux and heat generation or absorption. Srivastava et al. [31] have explored magneto-convection in an anisotropic porous layer with the Soret effect. Siddiqui and Mirza [32] investigated the magnetohydrodynamic free convection flows of a viscoelastic fluid in a porous medium with a variable permeability heat source and chemical reaction. Magnetic buoyancy instability and the anelastic approximation: regime of validity and relationship with compressible and Boussinesq descriptions are examined by Wilczynski, Hughes and Kersale [33]. They attempted to establish a connection between the descriptions of magnetic buoyancy in the compressible, anelastic, and boussinesq systems in their work. Additionally, it was demonstrated that magnetic buoyancy can be incorporated under both the anelastic and boussinesq approximations by combining a weak field with a strong gradient or, conversely, a strong field with a weak gradient. With specific governing equations, each has an asymptotically consistent reduction. Recent investigations in the field of MHD can be found in [34–38].

In light of the work previously mentioned and motivated by the work of [11] and [22], we are curious to see the impact of magnetic field and chemical reaction on the thermal convection of couple stress liquid, as the above mentioned work is studied without taking magnetic field into consideration, which currently has many applications in real life. Here, we try to analyse the stability criteria of themosolutal magneto-convection in couple stress liquid (in the absence of a body couple) using both linear and non-linear cases in this manuscript.

The outline of the paper is as follows: In Sect. 2, we give a brief mathematical model of a physical problem. Linear stability analysis, realistic as well as non-realistic boundary conditions, and oscillatory convection are reported in Sect. 3. In Sect. 4, a weakly non-linear theory with heat and mass transfer is covered. In Sect. 5, results and discussion are presented. The analysis is finished with a few key points in Sect. 6.

2. Mathematical Model

2.1. Physical Domain

We consider a couple-stress liquid of depth d, confined between two parallel horizontal planes at z = 0 and z = d, under the influence of an externally imposed constant magnetic field $\boldsymbol{\mathcal{H}_b} = \mathcal{H}_b\hat{\boldsymbol{k}}$. A cartesian frame of reference is chosen with the origin in the lower boundary and horizontal component x and vertical component z increasing upwards. The surfaces are stretched indefinitely in both x and y directions while maintaining a consistent temperature gradient ΔT and salinity gradient $\Delta\boldsymbol{\mathcal{C}}$ across the layer. We

are assuming that chemical equilibrium is maintained at the boundaries and that the Oberbeck-Boussinesq approximation is applied to account for the effect of density variations.

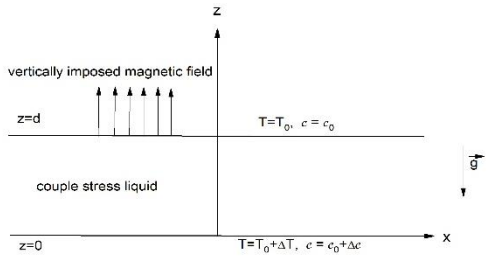

Fig. 1. Physical configuration of the problem considered.

2.2. Governing Equations

In the absence of a body couple, the continuity and momentum equations governing the motion of an incompressible couple stress fluid are given by [1]

$$\nabla . V = 0 \tag{1}$$

$$\rho_f \left[\frac{\partial V}{\partial t} + (V.\nabla)V\right] + \nabla P - \mu\nabla^2 V + \mu_1\nabla^4 V - \rho g - \mu_m(\mathcal{H}.\nabla)\mathcal{H} = 0. \tag{2}$$

The advection diffusion equations are used to describe the movement of heat and solute, according to Phillips [39]

$$\gamma\frac{\partial \mathrm{T}}{\partial \mathrm{t}} + (V.\nabla)T = \kappa_T\nabla^2 T \tag{3}$$

$$\frac{\partial \mathcal{C}}{\partial t} + (V.\nabla)\mathcal{C} = \kappa_{\mathcal{C}}\nabla^2\mathcal{C} + k\big(\mathcal{C}_{eq}(T) - \mathcal{C}\big) \tag{4}$$

$$\nabla.\mathcal{H} = 0 \tag{5}$$

$$\frac{\partial \mathcal{H}}{\partial t} + V.\nabla\mathcal{H} - \mathcal{H}.\nabla V = \Lambda\nabla^2\mathcal{H} \tag{6}$$

All the above mentioned variables are described in nomenclature at the end of the paper. The relation between the reference density, temperature, and salinity is given by

$$\rho = \rho_0[1 - \beta_T(T - T_0) + \beta_{\mathcal{C}}(\mathcal{C} - \mathcal{C}_0)] \tag{7}$$

The appropriate boundary conditions for temperature, solute, and magnetic field are:

$$T = T_0 + \Delta T \text{ at } z = 0 \text{ and } T = T_0 \text{ at } z = d\,, \tag{8}$$

$$\mathcal{C} = \mathcal{C}_0 + \Delta\mathcal{C} \text{ at } z = 0 \text{ and } \mathcal{C} = \mathcal{C}_0 \text{ at } z = d\,, \tag{9}$$

$$\boldsymbol{\mathcal{H}}\times\hat{k} = 0 \text{ at z = 0, } d \tag{10}$$

2.3. Basic State

Following [22], we have considered the equilibrium solute concentration as a linear function of temperature i.e. $\mathcal{C}_{eq}(T) = \mathcal{C}_0 + \varphi(T - T_0)$, where $\varphi = \frac{\mathcal{C}_l - \mathcal{C}_u}{T_l - T_u} = \frac{\Delta\mathcal{C}}{\Delta T}$. The value of φ may be positive i.e. the solubility increases with temperature (i.e. $\varphi > 0$) or negative i.e. the solubility decreases with temperature (i.e. $\varphi < 0$). In this paper, we have considered the case $\varphi > 0$.

The basic state of the fluid is assumed to be quiescent, and is given by

$$\begin{aligned} V_b = (0,0,0), P = P_b(z), T = T_b(z), \mathcal{C} \\ = \mathcal{C}_b(z) = \mathcal{C}_{eq}(T_b), \rho \\ = \rho_b(z), \mathcal{H}_b = \mathcal{H}_b\hat{k} \end{aligned} \tag{11}$$

Using (11) in Eqs. (1) – (7) yield

$$\frac{dp_b}{dz} = -\rho_b g, \frac{d^2T_b}{dz^2} = 0, \frac{d^2\mathcal{C}_b}{dz^2} = 0 \tag{12}$$

The basic state solution for temperature and solutal fields are given by:-

$$T_b(z) = T_l - \Delta T\frac{z}{d}, \mathcal{C}_b(z) = \mathcal{C}_l - \Delta\mathcal{C}\frac{z}{d} \tag{13}$$

2.4. Perturbed State

On the basic state, we superpose perturbation in the form:

$$\begin{aligned} V = V_b(z) + V'(x,y,z,t), T \\ = T_b(z) + T'(x,y,z,t), \mathcal{C} \\ = \mathcal{C}_b(z) + \mathcal{C}'(x,y,z,t), P \\ = P_b(z) + P'(x,y,z,t), \rho \\ = \rho_b(z) + \rho'(x,y,z,t), \mathcal{H} \\ = \mathcal{H}_b + \mathcal{H}'(x,y,z,t) \end{aligned} \tag{14}$$

Where primes indicate perturbations. Introducing (14) in Eqs. (1)–(6), and using basic state from Eqn. (12), we obtain

$$\nabla . V' = 0, \tag{15}$$

$$\rho_f\left[\frac{\partial V'}{\partial t} + (V'.\nabla)V'\right] + \nabla P' - \mu\nabla^2 V' + \mu_1\nabla^4 V' - \rho_0 g(T'\beta_T - \mathcal{C}'\beta_{\mathcal{C}}) - \mu_m H_b\frac{\partial \mathcal{H}'}{\partial z} = 0, \tag{16}$$

$$\gamma\frac{\partial T'}{\partial t} + (V'.\nabla)T' - w'\frac{\Delta T}{d} = \kappa_T\nabla^2 T', \tag{17}$$

$$\gamma\frac{\partial \mathcal{C}}{\partial t} + (V'.\nabla)\mathcal{C}' - w'\frac{\Delta\mathcal{C}}{d} = \kappa_{\mathcal{C}}\nabla^2\mathcal{C}' + k\big(\mathcal{C}_{eq}(T') - \mathcal{C}'\big), \tag{18}$$

$$\nabla.\mathcal{H}' = 0, \tag{19}$$

$$\frac{\partial \mathcal{H}}{\partial t} + (V'.\nabla)\mathcal{H}' - (\mathcal{H}'.\nabla)V' - \mathcal{H}_b\frac{\partial V'}{\partial z} = \Lambda\nabla^2\mathcal{H}'. \tag{20}$$

We non-dimensionalized the Eqs. (15) – (20) using following transformations

$$(x,y,z) = d(x^*,y^*,z^*), t = \frac{d^2}{\kappa_T}t^*, (u',v',w')$$
$$= \frac{\kappa_T}{d}(u^*,v^*,w^*), P' = \frac{\mu\kappa_\tau}{K_z}P^*, \mathcal{H}' \quad (21)$$
$$= \mathcal{H}_b\mathcal{H}^*, T' = (\Delta T)T^*, \mathcal{C}' = (\Delta\mathcal{C})\mathcal{C}^*,$$

then eliminate the pressure from the momentum transport Eqn. (16) by taking curl twice and arrive at the vorticity transport equation. The non-dimensional form of the vorticity and the heat transport equations are obtained in the form

$$\frac{1}{Pr}\left[\frac{\partial(\nabla^2 V)}{\partial t}\right] - (1 - C\nabla^2)\nabla^4 V - Ra_T\nabla_1^2 T + Ra_S\nabla_1^2\mathcal{C} - QP_m\frac{\partial(\nabla^2\mathcal{H})}{\partial z} = 0, \quad (22)$$

$$\gamma\frac{\partial T}{\partial t} + (V.\nabla)T - w = \left(\eta\nabla_1^2 + \frac{\partial^2}{\partial z^2}\right)T, \quad (23)$$

$$\frac{\partial\mathcal{C}}{\partial t} + (V.\nabla)\mathcal{C} - w = \frac{1}{Le}\nabla^2\mathcal{C} + \chi(T - \mathcal{C}), \quad (24)$$

$$\frac{\partial\mathcal{H}}{\partial t} + (V.\nabla)\mathcal{H} - (\mathcal{H}.\nabla)V - \frac{\partial V}{\partial z} = P_m\nabla^2\mathcal{H}. \quad (25)$$

where the non-dimensional parameters, $Pr = \frac{\mu}{\kappa_T\rho_f}$ is Prandtl number, $C = \frac{\mu_1}{\mu d^2}$ is Couple stress parameter, $Ra_T = \frac{\rho_0\beta_T\Delta T g d^3}{\mu\kappa_T}$ is Rayleigh number, $Ra_S = \frac{\rho_0\beta_\mathcal{C}\Delta\mathcal{C} g d^3}{\mu\kappa_T}$ is solutal Rayleigh number, $Q = \frac{\mu_m\mathcal{H}_b^2 d^2}{\rho_0\upsilon\upsilon_m}$ is Chandrashekhar number, P_m=$\frac{\upsilon_m}{\kappa_T}$ is magnetic Prandtl number, χ=$\frac{\kappa d^2}{\kappa_T}$ is Damköhler number and Le=$\frac{\kappa_T}{\kappa_\mathcal{C}}$ is Lewis number.

The boundaries of horizontal infinite plates can be considered either rigid or free. For rigid boundary surface on which no slip occurs [40], given as $w = \frac{\partial w}{\partial z} = \frac{\partial\mathcal{H}_z}{\partial z} = T = \mathcal{C} = 0$, and for free boundary surface on which no tangential stresses occurs, given by

$$w = \frac{\partial^2 w}{\partial z^2} = \frac{\partial\mathcal{H}_z}{\partial z} = T = \mathcal{C} = 0. \quad (26)$$

3. Linear Stability Analysis

Taking vertical component and neglecting non-linear terms from Eqs. (22)-(25) we get

$$\frac{1}{Pr}\left[\frac{\partial(\nabla^2 w)}{\partial t}\right] - (1 - C\nabla^2)\nabla^4 w - Ra_T\nabla_1^2 T + Ra_S\nabla_1^2\mathcal{C} - QP_m\frac{\partial(\nabla^2\mathcal{H}_z)}{\partial z} = 0, \quad (27)$$

$$\left(\gamma\frac{\partial}{\partial t} - \eta\nabla_1^2 - \frac{\partial^2}{\partial z^2}\right)T - w = 0, \quad (28)$$

$$\left(\frac{\partial}{\partial t} - \frac{1}{Le}\nabla^2 + \chi\right)\mathcal{C} - \chi T - w = 0, \quad (29)$$

$$\left(\frac{\partial}{\partial t} - P_m\nabla^2\right)\mathcal{H}_z = \frac{\partial w}{\partial z}. \quad (30)$$

Combing Eqs. (27) and (30), we get

$$\left[\frac{1}{P_r}\frac{\partial}{\partial t}\left(\frac{\partial}{\partial t} - P_m\nabla^2\right) - (1 - C\nabla^2)(\frac{\partial}{\partial t} - P_m\nabla^2)\nabla^2\right]\nabla^2 w - Ra_T\nabla_1^2\left(\frac{\partial}{\partial t} - P_m\nabla^2\right)T + Ra_S\nabla_1^2\left(\frac{\partial}{\partial t} - P_m\nabla^2\right)\mathcal{C} - QP_m\nabla^2\frac{\partial^2 w}{\partial z^2} = 0 \quad (31)$$

Using linear stability theory, we can predict marginal and oscillatory thresholds. Assuming the solutions to be periodic waves of the forms;

$$\begin{pmatrix} w \\ T \\ \mathcal{C} \end{pmatrix} = \begin{pmatrix} W(z) \\ \Theta(z) \\ \Phi(z) \end{pmatrix} e^{i(lx+my)+\sigma t} \quad (32)$$

where W, Θ and Φ are the amplitudes of stream function, temperature and concentration field, l and m are horizontal wave number and σ (a complex quantity) is the growth rate.

Substituting (32) in Eqs. (31), (28), and (29), we get

$$\left[\frac{\sigma}{Pr} - \left(1 - C(D^2 - a^2)\right)(D^2 - a^2)\right] * (D^2 - a^2)W + a^2 Ra_T\Theta - a^2 Ra_S\Phi - \frac{QP_m(D^2-a^2)D^2 W}{(\sigma - P_m(D^2-a^2))} = 0, \quad (33)$$

$$-\mathrm{W} + (\gamma\sigma + \eta a^2 - D^2)\Theta = 0, \quad (34)$$

$$-\mathrm{W} - \chi\Theta + \left(\sigma - \frac{D^2-a^2}{Le} + \chi\right)\Phi = 0. \quad (35)$$

where $D = \frac{d}{dz}$ and $a^2 = l^2 + m^2$.

The corresponding boundary condition (26) will be of the form

$$\mathrm{W} = \mathrm{DW} = \Theta = \Phi = 0 \quad \text{at} \quad z = 0,1, \quad (36)$$

on the rigid boundary and

$$\mathrm{W} = D^2\mathrm{W} = \Theta = \Phi = 0 \quad \text{at} \quad z = 0,1. \quad (37)$$

on the free boundary.

3.1. A Comparative Study

We solve the above eigenvalue problem for different boundary conditions and compare the results for all boundary conditions in the stationary case (i.e., σ= 0). For realistic boundary

conditions (R/R, F/R, and R/F), the above set of equations is solved numerically [41], whereas for non-realistic boundary conditions (F/F), exact solutions are obtained.

3.1.1. Realistic Boundary Conditions

In this case, the eigenvalue problem for R/R boundary conditions

$$W = DW = \Theta = \Phi = 0 \text{ at } z = 0,1. \tag{38}$$

R/F boundary conditions

$$W = DW = \Theta = \Phi = 0 \quad \text{at } z = 0, \tag{39}$$

$$\mathrm{W} = D^2\mathrm{W} = \Theta = \Phi = 0 \text{ at } z = 1. \tag{40}$$

and F/R boundary conditions

$$\mathrm{W} = D^2\mathrm{W} = \Theta = \Phi = 0 \text{ at } z = 0, \tag{41}$$

$$W = DW = \Theta = \Phi = 0 \quad \text{at } z = 1, \tag{42}$$

are solved. We use the Galerkin technique for solving the resulting eigenvalue problem for the above three types of boundary conditions. In this technique, the test (weighted) functions are the same as the base (trial) functions. Initially, the variables are written as a linear combination of basis functions as

$$W = \sum_{i=1}^{n} A_i W_i, \ \Theta = \sum_{i=1}^{n} B_i \Theta_i, \ \Phi = \sum_{i=1}^{n} C_i \Phi_i, \tag{43}$$

where $A_i, B_i \text{ and } C_i$ are constants and the basis functions W_i, Θ_i and Φ_i are represented by power series (will describe in (49), (50) and (51)), satisfy the corresponding boundary conditions.

Substituting (43) into (33)-(35), multiplying the resulting momentum equation by W_j (z), energy equation by Θ_j (z) and solutal equation by Φ_j (z), performing the integration by parts with respect to z between z = 0 and z = 1 and using the boundary conditions, leads to the following system of linear homogeneous algebraic equations

$$D_{ji}A_i + E_{ji}B_i + F_{ji}C_i = 0, \tag{44}$$

$$H_{ji}A_i + J_{ji}B_i = 0, \tag{45}$$

$$K_{ji}A_i + L_{ji}B_i + M_{ji}C_i = 0. \tag{46}$$

where,

$$\begin{aligned}
D_{ij} &= [3a^4P_m + 4a^6\mathrm{C}P_m + \mathrm{Q}P_m a^2]\,\langle \mathrm{D}W_j, \mathrm{D}W_i\rangle \\
&+ [3a^2P_m + 6\mathrm{C}P_m a^4 + \mathrm{QP} + \mathrm{m}]\,\langle D^2W_j, D^2W_i\rangle + \\
&[4a^2\mathrm{C}P_m + P_m]\,\langle D^3W_j, D^3W_i\rangle + \\
&\mathrm{C}P_m\langle D^4W_j, D^4W_i\rangle + [a^6P_m + a^8\mathrm{C}P_m]\,\langle W_j, W_i\rangle, \\
E_{ij} &= -[P_m a^4 Ra_T]\langle W_j, \Theta_i\rangle \\
&-[P_m a^2 Ra_T]\langle DW_j, \mathrm{D}\Theta_i\rangle, \\
F_{ij} &= -[P_m a^4 Ra_S]\langle W_j, \Phi_i\rangle \\
&+[P_m a^2 Ra_S]\langle DW_j, \mathrm{D}\Phi_i\rangle, \\
H_{ij} &= -\langle \Theta_j, \mathrm{W}_i\rangle, J_{ji} = \\
&[\eta a^2]\langle \Theta_j, \Theta_i\rangle + \langle \mathrm{D}\Theta_j, \mathrm{D}\Theta_i\rangle, \\
K_{ji} &= -\langle \Phi_j, \mathrm{W}_i\rangle, L_{ji} = -\chi\langle \Phi_j, \Theta_i\rangle, M_{ji} \\
&= \left[\frac{a^2}{Le} + \chi\right]\langle \Phi_j, \Phi_i\rangle + \frac{1}{Le}\langle \mathrm{D}\Phi_j, \mathrm{D}\Phi_i\rangle
\end{aligned} \tag{47}$$

here the inner product $\langle ... \rangle$ is defined as $\langle \dots \rangle = \int_0^1 (\dots) dz$

The above set of homogeneous algebraic equations can have a non-trivial solution if and only if

$$\begin{vmatrix} D_{ji} & E_{ji} & F_{ji} \\ H_{ji} & J_{ji} & 0 \\ K_{ji} & L_{ji} & M_{ji} \end{vmatrix} = 0 \tag{48}$$

For R/R boundaries, trial functions are:

$$\begin{aligned} W_i &= z^{i+1} + 2z^{i+2} + z^{i+3}, \\ \Theta_i &= \Phi_j = z^i - z^{i+1}, \end{aligned} \tag{49}$$

For R/F boundaries, trial functions are:

$$\begin{aligned} W_i &= 2z^{i+3} - 3z^{i+1} - 5z^{i+2}, \\ \Theta_i &= \Phi_j = z^i - z^{i+1}, \end{aligned} \tag{50}$$

and for F/R boundaries conditions, trial functions are:

$$\begin{aligned} W_i &= z^{i+4} + z^{i+2} - 2z^{i+3}, \\ \Theta_i &= \Phi_j = z^i - z^{i+1}. \end{aligned} \tag{51}$$

here (*i=1,2,3...n*).

From a rigorous numerical experiment, it has been found that the order of the polynomial, *n = 5* is sufficient to reach the required accuracy, which is shown in Tables 1 and 2.

Table 1. Comparison of results for different orders of Galerkin approximation for $\chi = 0.8$ for different values C

	n=2		n=3		n=4		n=5	
	Ra_T^C	a^C	Ra_T^C	a^C	Ra_T^C	a^C	Ra_T^C	a^C
C=0	40962	2.13	40962	2.13	40959	2.11	40959	2.11
C=1	1935702	2.32	1935700	2.32	1935697	2.29	1935697	2.29
C=1.5	2810800	1.94	2810800	1.94	2810800	1.94	2810800	1.94
C=2	3674898	2.11	3674898	2.11	3674895	2.08	3674895	2.08

Table 2. Comparison of results for different orders of Galerkin approximation for $\chi = 0.8$ for different values of Ra_S

	n=2		n=3		n=4		n=5	
	Ra_T^C	a^C	Ra_T^C	a^C	Ra_T^C	a^C	Ra_T^C	a^C
Ra_S=50	54809	2.02	54809	2.02	54809	2.02	54809	2.02
Ra_S=100	55233	2.04	55233	2.04	55232	2.03	55232	2.03
Ra_S=200	56078	2.05	56078	2.05	56076	2.05	56076	2.05
Ra_S=500	58608	2.13	58608	2.13	58607	2.11	58607	2.11

3.1.2. Non Realistic Boundary Conditions

We take the solution of Eqs. (33)-(35) satisfying the boundary condition for free-free (F/F) case:

$$[W(z), \Theta(z), \Phi(z)] = [W_0, \Theta_0, \Phi_0] \sin(n\pi z), \quad (n = 1,2,3, \dots). \tag{52}$$

Substituting Eqn. (52) into (33)-(35), we obtain a matrix equation considering n = 1

$$\begin{bmatrix} \zeta & \xi & \vartheta \\ -1 & \gamma\sigma + \alpha_1 & 0 \\ -1 & -\chi & \sigma + \alpha_2 + \chi \end{bmatrix} \begin{bmatrix} W_0 \\ \Theta_0 \\ \Phi_0 \end{bmatrix} = \begin{bmatrix} 0 \\ 0 \\ 0 \end{bmatrix}, \tag{53}$$

$\alpha = a^2 + \pi^2$, $\alpha_1 = \eta a^2 + \pi^2$, $\alpha_2 = \frac{a^2}{Le}$,

$\zeta = \left[\frac{\sigma\alpha}{Pr} + \alpha^2 + C\alpha^3\right](\sigma + P_m\alpha) + QP_m\pi^2\alpha$,

$\xi = -a^2 Ra_T(\sigma + P_m\alpha)$,

$\vartheta = -a^2 Ra_S(\sigma + P_m\alpha)$.

For non-trivial solution of W_0, Θ_0 and Φ_0, we need to make the determinant of the above matrix as zero, we get

$$Ra_T = \left[\frac{\sigma\alpha}{Pr} + \alpha^2(1 + C\alpha) + \frac{QP_m\pi^2\alpha}{(\sigma + P_m\alpha)}\right]\frac{\nu\sigma + \alpha_1}{a^2} + \frac{Ra_S(\chi + \gamma\sigma + \alpha_1)}{(\sigma + \alpha_2 + \chi)}. \tag{54}$$

3.2. Stationary State

For the direct bifurcation (i.e., steady onset), we have $\sigma = 0$ at the the margin of stability. Then, the Rayleigh number at which marginally stable steady mode exists, becomes

$$Ra_T^{st} = [\alpha^2(1 + C\alpha) + Q\pi^2]\frac{\alpha_1}{a^2} + Ra_S\frac{(\chi + \alpha_1)}{(\chi + \alpha_2)} \tag{55}$$

In the absence of Q = 0 the Eqn. (55) reduces to

$$Ra_T^{st} = [\alpha^2(1 + C\alpha)]\frac{\alpha_1}{a^2} + Ra_S\frac{(\chi + \alpha_1)}{(\chi + \alpha_2)}, \tag{56}$$

when Ra_S = C = 0, Eqn. (56) reduces to

$$Ra_T^{st} = \frac{(a^2 + \pi^2)^2(\eta a^2 + \pi^2)}{a^2}, \tag{57}$$

further if porous media is isotropic in mechanical and thermal properties, i.e. $\eta = 1$, then Eqn. (57) becomes

$$Ra_T^{st} = \frac{(a^2 + \pi^2)^3}{a^2}. \tag{58}$$

which has the critical value Ra_T^{st},c = 657.5 for $a_c = \frac{\pi}{\sqrt{2}}$, as obtained by [40].

3.3. Oscillatory State

The growth rate σ is in general a complex quantity such that $\sigma = \sigma_r + i\omega$. The system with $\sigma_r < 0$ is always stable, while for $\sigma_r > 0$ it will become unstable. For neutral stability state $\sigma_r = 0$, We put $\sigma = i\omega$ (ω is real) in Eqn. (54) and obtain

$$Ra_T = \Pi_1 + (i\omega)\Pi_2 \tag{59}$$

The expression for Π_1 is given by

$\Pi_1 = \mathcal{D}_1 + \mathcal{D}_2 + \mathcal{D}_3$,

where

$$\mathcal{D}_1 = (M_5 - M_6\omega^2)\left[1 + \frac{M_2}{M_3 + \omega^2}\right],$$

$$\mathcal{D}_2 = \omega^2\frac{M_1M_4}{M_3 + \omega^2},$$

$$\mathcal{D}_3 = \frac{M_9 + M_{10}\omega^2}{M_8 + \omega^2} \quad .$$

Since Ra_T is a physical quantity, it must be real. Hence, from Eqn. (59) it follows that either $\omega = 0$ (steady onset) or $\Pi_2 = 0$ ($\omega \neq 0$, oscillatory onset). For oscillatory onset $\Pi_2 = 0$ ($\omega \neq 0$) and this gives a dispersion relation of the form

$$\mathcal{B}_1(\omega^2)^2 + \mathcal{B}_2(\omega^2) + \mathcal{B}_3 = 0 \tag{60}$$

where the constants

$$\mathcal{B}_1 = M_1 + M_4M_6,$$

$$\mathcal{B}_2 = M_1M_3 + M_1M_8 + M_1M_2 - M_4M_5 + M_4M_6M_8 + M_7,$$

$$\mathcal{B}_3 = M_1M_3M_8 + M_1M_2M_8 - M_4M_5M_8 + M_3M_7$$

Now Eqn. (59) with $\Pi_2 = 0$, gives oscillatory Rayleigh number Ra_T^{osc} at the margin of stability as

$$Ra_T^{osc} = \Pi_1 \tag{61}$$

Also for the oscillatory convection to occur, ω^2 must be positive. The symbols $M_1, M_2, M_3, M_4, M_5, M_6, M_7, M_8, M_9, M_{10}$ and Π_2 are defined in Appendix.

4. Weakly Non-Linear Theory

In this part, we take into account the non-linear analysis using a truncated Fourier series representation with two terms. Although the linear stability analysis is sufficient to determine the stability condition of the motionless solution and the associated eigenfunctions qualitatively describing the convective flow, it is unable to reveal the values of the convection amplitudes or the rate of heat and mass transfer. We conduct the non-linear analysis in order to obtain this additional information, which is helpful to comprehend the physical process with the least amount of mathematical analysis and is a step towards comprehending the complete non-linear problem.

Introducing stream functions ψ and ϕ as

$$u = \frac{\partial \psi}{\partial z}, w = -\frac{\partial \psi}{\partial x}, \mathcal{H}_x = \frac{\partial \phi}{\partial z} \text{ and } \mathcal{H}_z = -\frac{\partial \phi}{\partial x}.$$

Into vertical component of Eqs. (22)-(25), we obtain

$$-\frac{1}{Pr}\frac{\partial}{\partial t}\left(\frac{\partial^2}{\partial x^2} + \frac{\partial^2}{\partial z^2}\right)\psi + \left(1 - C\left(\frac{\partial^2}{\partial x^2} + \frac{\partial^2}{\partial z^2}\right)\right)\left(\frac{\partial^4}{\partial x^4} + \frac{\partial^4}{\partial z^4}\right)\psi - Ra_T\frac{\partial T}{\partial x} + Ra_S\frac{\partial \mathcal{C}}{\partial x} + QP_m\left(\frac{\partial^2}{\partial x^2} + \frac{\partial^2}{\partial z^2}\right)\frac{\partial \phi}{\partial z} = 0, \tag{62}$$

$$\frac{\partial \psi}{\partial x} + \left(\upsilon\frac{\partial}{\partial t} - \eta\frac{\partial^2}{\partial x^2} - \frac{\partial^2}{\partial z^2}\right)T - \frac{\partial(\psi,T)}{\partial(x,z)} = 0, \tag{63}$$

$$\frac{\partial \psi}{\partial x} + \left(\frac{\partial}{\partial t} - \frac{1}{Le}\left(\frac{\partial^2}{\partial x^2} + \frac{\partial^2}{\partial z^2}\right) + \chi\right)\mathcal{C} - \chi T - \frac{\partial(\psi,\mathcal{C})}{\partial(x,z)} = 0, \tag{64}$$

$$\frac{\partial \phi}{\partial t} - \frac{\partial(\psi,\phi)}{\partial(x,z)} - \frac{\partial \psi}{\partial z} - P_m\left(\frac{\partial^2}{\partial x^2} + \frac{\partial^2}{\partial z^2}\right)\phi = 0. \tag{65}$$

A minimal double Fourier series which describes the finite amplitude steady-state convection is given by

$$\psi = A_1(t)sin(\pi ax)sin(\pi z), \tag{66}$$

$$T = B_1(t)\cos(\pi ax)\sin(\pi z) + B_2(t)sin(2\pi z), \tag{67}$$

$$\mathcal{C} = C_1(t)\cos(\pi ax)\sin(\pi z) + C_2(t)\,sin(2\pi z) \tag{68}$$

$$\phi = D_1(t)\sin(\pi ax)\cos(\pi z) + D_2(t)sin(2\pi ax). \tag{69}$$

Where the amplitudes A_1(t), B_1(t), B_2(t), C_1(t), C_2(t), D_1(t) and D_2(t) are to be determined from the dynamics of the system. Substituting Eqs. (66) – (69) into Eqs. (62)-(65) and equating the coefficients of like terms, we obtain the following non-linear autonomous system of differential equations

$$\frac{P_1}{Pr}\frac{dA_1}{dt} = -(P_2 + CP_3)A_1 - \pi aRa_TB_1 + \pi aRa_SC_1 - QP_mP_4D_1, \tag{70}$$

$$\frac{dB_1}{dt} = -\left(\frac{\pi a}{\gamma}\right)A_1 - \left(\frac{\eta P_1}{\gamma}\right)B_1 - \frac{2\pi a^2}{\gamma}A_1B_2, \tag{71}$$

$$\frac{dB_2}{dt} = -\left(\frac{4\pi^2}{\gamma}\right)B_2 + \left(\frac{a\pi^2}{2\gamma}\right)A_1B_1, \tag{72}$$

$$\frac{dC_1}{dt} = \chi B_1 - 2\pi^2 aA_1C_2 - \left(\frac{\pi^2a^2+\pi^2}{Le} + \chi\right)C_1 - \pi aA_1, \tag{73}$$

$$\frac{dC_2}{dt} = -\left(\frac{4\pi^2}{Le} + \chi\right)C_2 + \left(\frac{a\pi^2}{2}\right)A_1C_1 + \chi B_2, \tag{74}$$

$$\frac{dD_1}{dt} = -P_mP_1D_1 + \pi^2 aA_1D_2 + \pi A_1, \tag{75}$$

$$\frac{dD_2}{dt} = -4P_m\pi^2a^2D_2 - \frac{\pi^2 a}{2}A_1D_1. \tag{76}$$

where,

$P_1 = (\pi^2a^2 + \pi^2)$,
$P_2 = (\pi^4a^4 + \pi^4)$,
$P_3 = (\pi^6a^6 + \pi^6), P_4 = \pi^3(a^2 + 1)$.

From qualitative predictions we look into the possibility of an analytical solution. In the case of steady motion, Eqs. (70) – (76) can be solved in closed from. Setting the left hand side equal to zero we get

$$(P_2 + CP_3)A_1 + \pi a Ra_T B_1 - \pi a Ra_S C_1 + QP_m P_4 D_1 = 0, \quad (77)$$

$$(\pi a)A_1 + (\eta P_1)B_1 + 2\pi^2 a A_1 B_2 = 0, \quad (78)$$

$$\left(\frac{4\pi^2}{Le} + \chi\right)C_2 - \left(\frac{\pi^2 a}{2}\right)A_1 C_1 - \chi B_2 = 0, \quad (79)$$

$$\chi B_1 + 2\pi^2 a A_1 C_2 + \left(\frac{\pi^2 a^2 + \pi^2}{Le} + \chi\right)C_1 + \pi a A_1 = 0, \quad (80)$$

$$\left(\frac{4\pi^2}{Le} + \chi\right)C_2 - \left(\frac{a\pi^2}{2}\right)A_1 C_1 - \chi B_2 = 0, \quad (81)$$

$$P_m P_1 D_1 - \pi^2 a A_1 D_2 - \pi A_1 = 0, \quad (82)$$

$$4P_m \pi^2 a^2 D_2 + \frac{\pi^2 a}{2} A_1 D_1 = 0. \quad (83)$$

We express B_1, B_2, C_1, C_2, D_1 and D_2 in terms of A_1, for this we use Eqs. (78) – (83) , and substituting these in Eqn. (77) with $\frac{A_1^2}{8} = M$ we get

$$a_0 M^3 + b_0 M^2 + c_0 M + d_0 = 0. \quad (84)$$

where

$a_0 = m_1 p_2 p_4 p_8, b_0 = m_1 m_6 p_4 p_8 + m_1 m_{11} p_2 p_8 + m_1 m_{16} p_2 p_4 - p_1 p_4 p_8 + p_2 p_3 p_8 - \frac{P_5 P_8}{P_6} + p_2 p_4 p_7, c_{0=} m_1 m_6 m_{11} p_8 + m_1 m_6 m_{16} p_4 + m_1 m_{11} m_{16} p_2 - m_{11} p_1 p_8 - m_{16} p_1 p_4 - \frac{m_{16} p_5}{p_6} + p_8 p_9 + m_6 p_4 p_7 + m_{11} p_2 p_7 + p_3 m_6 p_8 + p_3 p_2 m_{16}, d_0 = m_1 m_6 m_{11} m_{16} - p_1 m_{11} m_{16} + p_9 m_{16} + m_6 m_{11} p_7 + p_3 m_6 m_{16}.$

The symbols $m_1, m_2, m_3, m_4, m_5, m_6, m_7, m_8, m_9, m_{10}, m_{11}, m_{12}, m_{13}, m_{14}, m_{15}, m_{16}, m_{17}, m_{18}, m_{19}, p_1, p_2, p_3, p_4, p_5, p_6, p_7, p_8$ and p_9 are defined in Appendix.

4.1. Heat and Mass transports

It is a known fact that for higher values of the Rayleigh number, the onset of convection is generally governed by heat and mass transfer within the system. Consequently, here we are defining the Nusselt number and Sherwood number (following Srivastava and Bera [22]) as,

$$Nu = \frac{h}{\kappa_{T_z}\Delta T/d} = (1 - 2\pi B_2). \quad (85)$$

$$Sh = \frac{J}{\kappa_S \Delta \mathcal{C}/d} = (1 - 2\pi C_2). \quad (86)$$

where B_2, C_2 are found in terms of A_1. Substituting B_2, C_2 in Eqs. (85) and (86), we get

$$Nu = 1 + \left[\frac{16\pi m_5 m_9 M}{m_8(m_6 + 8p_2 M)}\right], \quad (87)$$

$$Sh = 1 + \frac{16\pi m_{10} m_{15} M}{m_{14}(m_{11}+8p_4 M)} + \frac{16\pi m_2 m_{12} m_{15} M}{m_{14}(m_{11}+8p_4 M)(m_6+8p_2 M)} + \frac{128\pi m_5 m_9 m_{12} m_{13} m_{15} M^2}{m_8 {m_{14}}^2 (m_{11}+8p_4 M)(m_6+8p_2 M)} - \frac{16\pi m_5 m_9 m_{12} M}{m_8 m_{14}(m_6+8p_2 M)} \quad (88)$$

5. Result and Discussion

5.1. Linear Stability Theory

Linear stability analysis is divided into two subsections: The first part is dedicated to a comparative study of stationary cases for different boundary conditions, and in the second part, we focus on stationary and oscillatory cases for the F/F boundary conditions.

5.1.1. Stationary Case (A Comparative Study)

Figures. 2–6 represent a comparative study of the stability criteria of different controlling parameters on the onset of convection for the different boundary conditions described above. We use $(Ra_S - {Ra_T}^C)$ plane to demonstrate the stability criteria.

Figure 2 illustrates the effect of magnetic field (Q) in the $(Ra_S - {Ra_T}^C)$ plane for different boundary conditions. It is clearly observed from the figure that the value of the critical Rayleigh number increases with an increasing value of Q. This indicates that the onset of convection delay i.e. stabilizes the system with an increasing value of Q. This phenomena can be explained due to fact that when the magnetic field strength permeating the medium is considerably strong, it induces viscosity into the fluid, and the magnetic lines are distorted by convection. Then these magnetic lines hinder the growth of disturbances, leading to the delay in the onset of instability. Stability criteria for different boundary conditions are listed in decreasing order as follows: F/F>F/R>R/R>R/F. This graph also shows that as Q increases, so does the slight increase in the $RaTC$ values between various boundary

conditions. From the figure, it can also be observed that with an increasing value of Ra_S, the value of $Ra_T{}^C$ also increases, indicating that the stability of the system increases. This is due to the fact that as the value of Ra_S increases, the value of concentration gradient (ΔC) increases, so heat diffuses with solute delay the onset of convection.

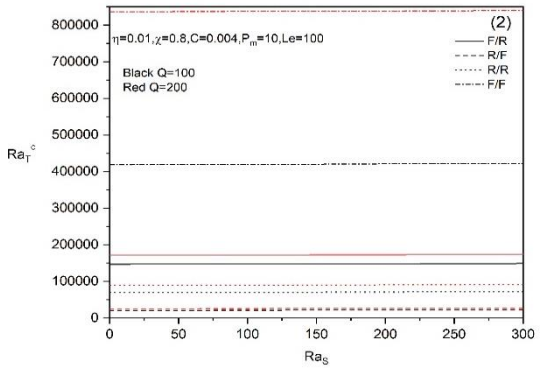

Fig. 2. Variation of Ra_T^c as a function of solutal Rayleigh number Ra_S for different values of Chandrashekhar number (Q) in (Ra_S, Ra_T^c) plane.

The impact of the Couple stress parameter (C) on the stability of the system is shown in Figure 3. We can easily observe that when the value of C rises, the stability of the system also rises, and hence its effect is to contract the size of convection cells. Since couple stress parameter and couple stress viscosity are inversely proportional to one another, this phenomenon can be explained physically by the fact that both increase with increasing couple stress parameter. Therefore, prandlt number grows due to an increase in couple stress viscosity, which is again directly proportional to Rayleigh number. The system is most stable for F/R boundary conditions and less stable for R/F boundaries. Additionally, as the value of C increases, the variation in $Ra_T{}^C$ values also increases across various boundary conditions.

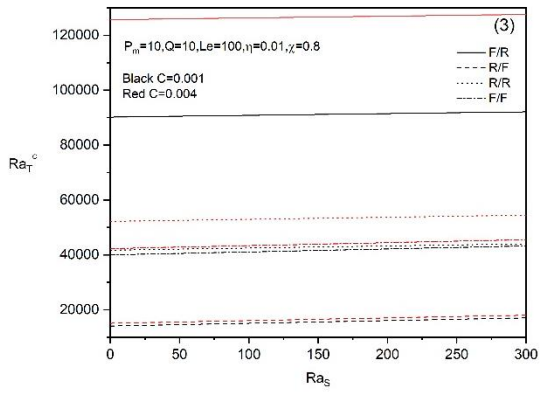

Fig. 3. Variation of Ra_T^c as a function of solutal Rayleigh number Ra_S for different values of Couple stress parameter (C) in (Ra_S, Ra_T^c) plane.

Figure 4. illustrates how the non-dimensional Damköhler number (χ) affects the system's stability. It is demonstrated that as χ increases, the stability of the system falls; for F/R boundaries, system is most stable and for R/F boundaries least among all four conditions. The physics behind this is that increasing the value of χ increases the chemical reaction rate, which causes a decrease in the value of the critical Rayleigh number. Also, the deviation in the values of $Ra_T{}^C$ among different boundary conditions decreases with an increase in the value of χ.

Figure 5. illustrates that the critical Rayleigh number $Ra_T{}^C$ increases slowly with an increase in the value of Ra_S but significantly increases with an increase in the value of the thermal anisotropic parameter η in the case of F/R boundaries when compared to R/R, R/F and F/F boundaries. Also, with the increase in value, of η, the stability of the system increases, and it is evident that F/R is the most stable and R/F is the least stable. It can be understood by the fact that η is basically the ratio of thermal permeability in the x-direction to the z–direction, so increasing the value of η depends on increasing thermal permeability in x-direction as thermal permeability in z-direction is fixed using other controlling parameters. As thermal permeability in x-direction increases, heat defuses horizontally, which delays the onset of convection.

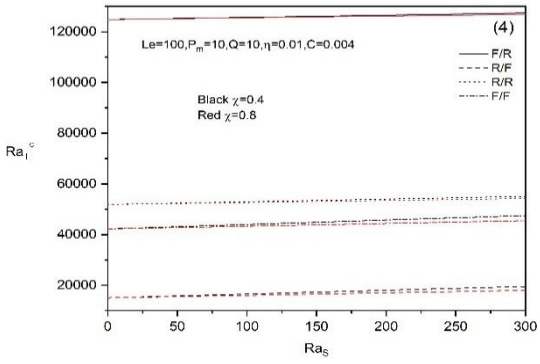

Fig. 4. Variation of Ra_T^c as a function of solutal Rayleigh number Ra_S for different values of Damköhler number (χ) in (Ra_S, Ra_T^c) plane.

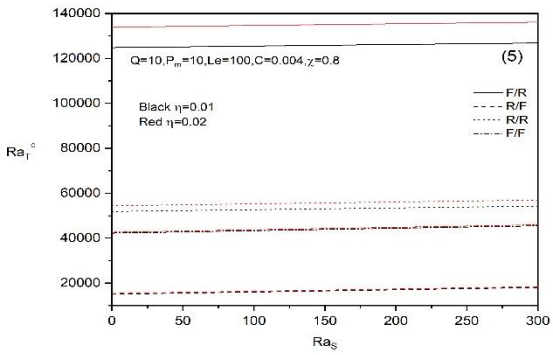

Fig. 5. Variation of Ra_T^c as a function of solutal Rayleigh number Ra_S for different values of thermal anisotropic parameter (η) in (Ra_S, Ra_T^c) plane.

Figure 6. displays the impact of the Lewis number (Le) on the stability of the system. As the value of Le grows, we can observe that the system is more stable. This is because the Lewis number is defined as the ratio of thermal diffusivity to mass diffusivity, but the impact of thermal diffusivity is not significant; hence, the effect of Lewis number is to advance the onset of convection. Consequently, they have the effect of contracting the size of the convection cells. Further, it is observed that $(Ra_T^C)_{F/R}>(Ra_T^C)_{R/R}>(Ra_T^C)_{F/F}>(Ra_T^C)_{R/F}$.

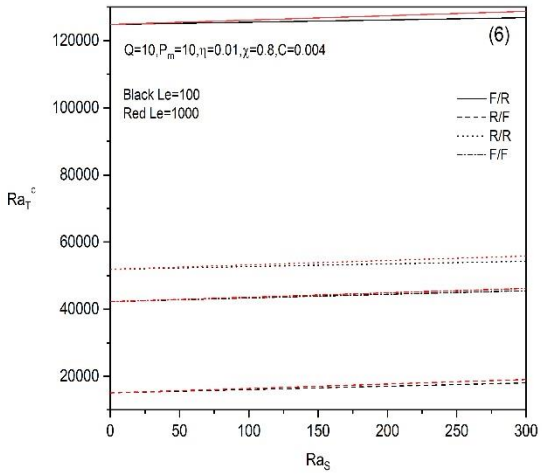

Fig. 6. Variation of Ra_T^c as a function of solutal Rayleigh number Ra_S for different values of Lewis number (Le) in (Ra_S, Ra_T^c) plane.

5.1.2. *Comparison Between Stationary and Oscillatory Convection (for F/F Case)*

Figures. 7-8 illustrates how the solutal Rayleigh number Ra_S, affects stationary and oscillatory convection in the (a, Ra_T^{st}) plane.

We can observe that raising Ra_S has the impact of raising the critical Rayleigh number as well as the corresponding wave number, showing that Ra_S has the effect of advancing the onset of convection. This figure plots the results of stationary and oscillatory convection on a plateform and compares their findings. In Figure 8. it has been observed that as Ra_S increases, the minimum Rayleigh number decreases, indicating that the system's stability is reduced by oscillatory convection. The behaviour of the solutal Rayleigh number is clear and consistent with the findings of [42].

It is interesting to observe that stationary and oscillatory convection are affected in opposite ways by the solutal Rayleigh number. The minimal critical Rayleigh number increases for stationary convection while decreasing for oscillatory convection as Ra_S values grow.

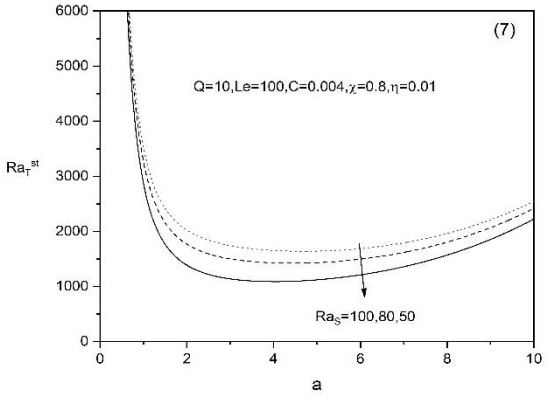

Fig. 7. Stationary neutral stability for different values of solutal Rayleigh number Ra_S in (a, Ra_T^{st}) plane.

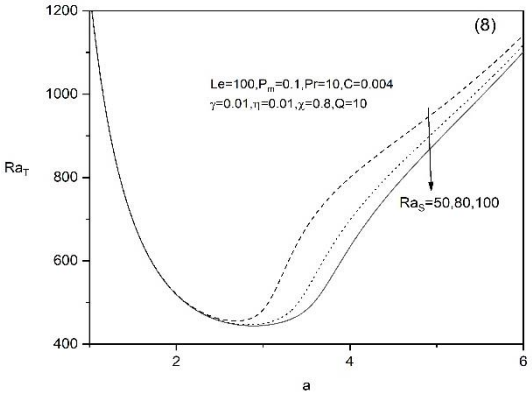

Fig. 8. Oscillatory neutral stability curves for different values of solutal Rayleigh number (Ra_S) in (a, Ra_T) plane.

5.1.3. *Oscillatory Convection (for F/F case):-*

Figures. 9-12 show graphs for various values of Couple stress parameter (C), Chandrashekhar number (Q), Damköhler number(χ) and ratio of heat capacities on heat transfer (γ) on the (a, Ra_T) plane for oscillatory convection. These neutral curves are topologically connected, which conforms to the linear stability criteria expressed in terms of the critical Rayleigh number. This leads one to the conclusion that a system is stable if its critical Rayleigh number is below it and unstable if it is above it.

When the values of the other parameters are fixed, Figures 9(a)-(b). show graphs for various values of C on the (a, Ra_T) and (a, ω^2) planes. Figure 9(a). revealed that as the value of C grows, the minimum value of the Rayleigh number also rises, suggesting that the couple stress parameter stabilises the system. To comprehend how this works, consider the definition of C. It should be noted that an increase in C indicates that the viscosity of couple stress has increased as well. Thus, the aforementioned result is predicted. For various values of C, the appropriate square of frequency is depicted in Figure 9(b). as a function of wave number. It can be seen that as C is reduced, the maximum value of frequency rises [22].

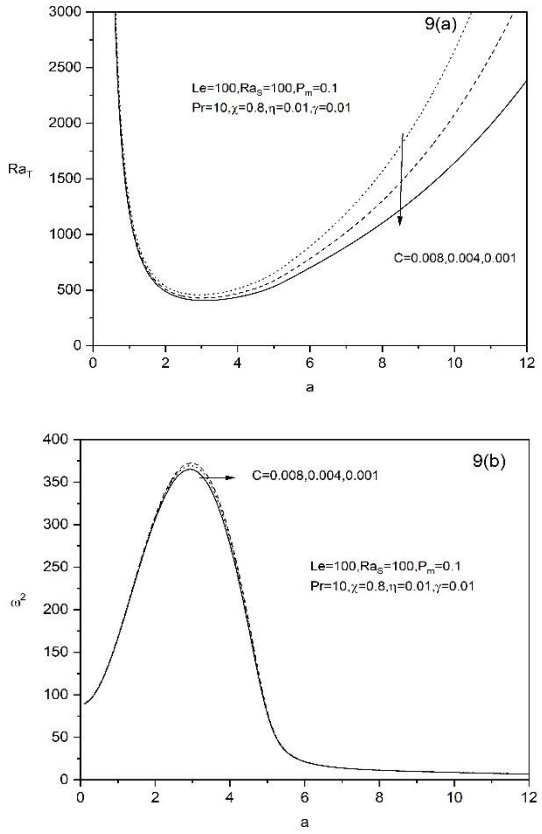

Fig. 9. Oscillatory neutral stability curves for different values of **9(a)** Couple stress parameter (C) in (a, Ra_T) plane **; 9(b)** Couple stress parameter (C) in (a, ω^2) plane.

Figure 10. shows graph on the (a, Ra_T) plane for various values of Chandrashekhar number Q when the values of other parameters are fixed. It is shown in Figure 10. and Table 3 that with an increase in Q, the minimum Rayleigh number rises, indicating that the system's stability is amplified. The relationship between thermal diffusivity and Chandrasekhar number is inverse; therefore, it makes sense. A lower thermal diffusivity means a higher buoyancy, which implies a higher Rayleigh number. Also, this result is in agreement with the results of [31].

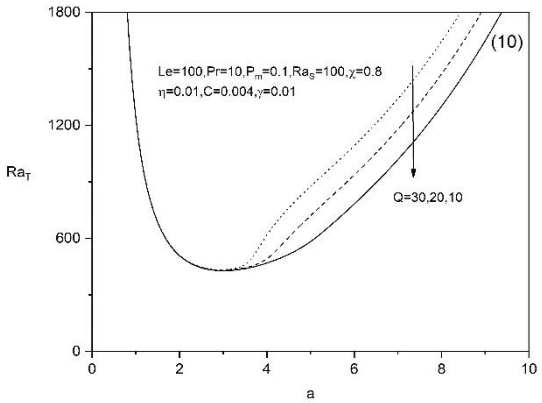

Fig. 10. Oscillatory neutral stability curves for different values of Chandrashekhar number (Q) in (a, Ra_T) plane.

Table 3. Variation of Ra_T with wave number a for different value of Q for oscillatory convection.

	Ra_T		
a	$Q = 10$	Q=20	Q=30
1	1230	1231.7	1232.3
2	508.0452	509.0886	509.9690
3	428.1112	430.3825	433.5097
4	469.0883	490.3406	617.6845
5	582.8854	720.1603	875.7899
6	782.7229	936.6037	1092.5

Figure 11. shows how the Damköhler number (χ) affects the oscillatory Rayleigh number on the (a, Ra_T) plane. As χ rises, the critical Rayleigh number lowers, showing that χ moves the onset of oscillatory convection forward, as shown in Figure 11. as well as in Table 4. The science underlying this behaviour is that the value of the Rayleigh number decreases as the value of χ (chemical reaction rate) increases. A brief look at the solute equation, where an additional reaction term has been introduced, can help to explain this. Since, increasing the value of chemical reactions, a displaced fluid particle's solute concentration will change and quickly equilibrate with the surrounding fluid. As a result, it reduces and eventually eliminates the energy source for the onset of oscillatory instability.

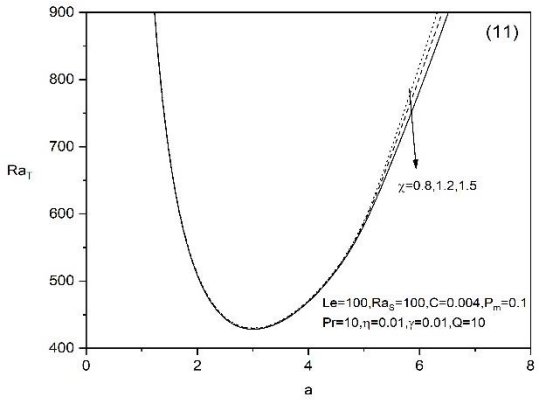

Fig. 11. Oscillatory neutral stability curves for different values of damköhler number(χ) in (a, Ra_T) plane.

Table 4. Variation of Ra_T with wave number a for different value of χ for oscillatory convection.

	Ra_T		
a	$\chi = 0.8$	χ=1.2	χ=1.5
1	1235	1233	1230
2	510.3778	509.3729	508.0452
3	429.9820	429.1820	428.1112
4	471.2979	470.3674	469.0883
5	588.8700	586.4477	582.8854
6	820.8040	803.4479	782.7229

The impact of the ratio of heat capacities on heat transfer γ on the stability of the system is shown in Figure 12. in the (a, Ra_T) plane. It has been shown in Figure 12. that as the value of γ, increased, the lowest Rayleigh number also rises, indicating that γ increases system stability. We will use the definition of the dimensionless inter-phase heat transfer coefficient to describe this phenomenon. Increasing inter-phase heat transfer coefficients mean heat transfer in fluids increases. So, heat is involved in transferring fluid from one phase to another phase. Hence, it stabilizes the system.

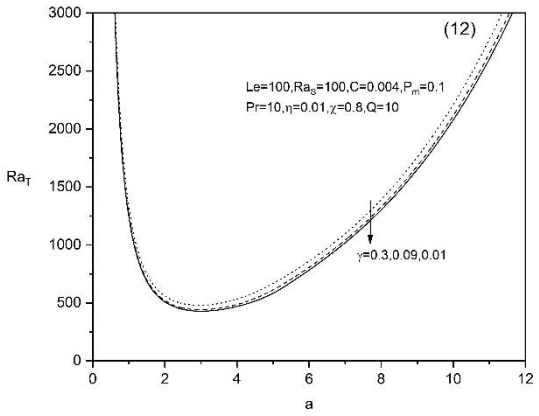

Fig. 12. Oscillatory neutral stability curves for different values of ratio of heat capacities on heat transfer (γ) in (a, Ra_T) plane.

5.2. Weakly Non-Linear Stability Analysis

Based on the smallest possible representation of a truncated Fourier series, which describes the possibility for motions with finite amplitudes, we additionally determine the quantity of heat and mass transfer in non-linear mode. Weakly non-linear stability analysis is divided into two parts: the steady case (time independent) and the unsteady case (time dependent).

5.2.1. Steady Case (for F/F Boundaries)

Determining the flow of heat and mass across the layer is crucial in the study of thermosolutal magneto-convection. In this case, the impact on heat and mass transfer makes it easier to spot the onset of convection as the Rayleigh number rises. Nusselt number (Nu) and Sherwood number (Sh), which indicate the ratio of heat or mass transmitted across the layer to the heat or mass transported by conduction alone, respectively, provide the amount of heat and mass transfer across the layer.

For different values of the Chandrashekhar number (Q), Couple stress parameter (C), Lewis number (Le), and solutal Rayleigh number (Ra_S) for the steady case of non-linear theory, the effects of Ra_T on Nu and Sh are shown in Figures. 13–16. It is evident that as Ra_T increases past its critical point, the transmission of mass and heat increases significantly. This trend persists until Ra_T reaches a certain threshold value. However, once Ra_T is raised even further, Nu and Sh approach a steady state. In each case, it is also found that the value of Nusselt number Nu is greater than the value of Sherwood number Sh.

Figures. 13(a)-(b) depict the impact of the Chandrashekhar number (Q) for fixed values of other parameters in the (Ra_T , Nu) and (Ra_T, Sh) planes. From these figures, it can be observed that the Nusselt and Sherwood numbers rise together with the rise in the value of the Chandrashekhar number (Q) and, after some point, become almost constants. Convection has therefore advanced.

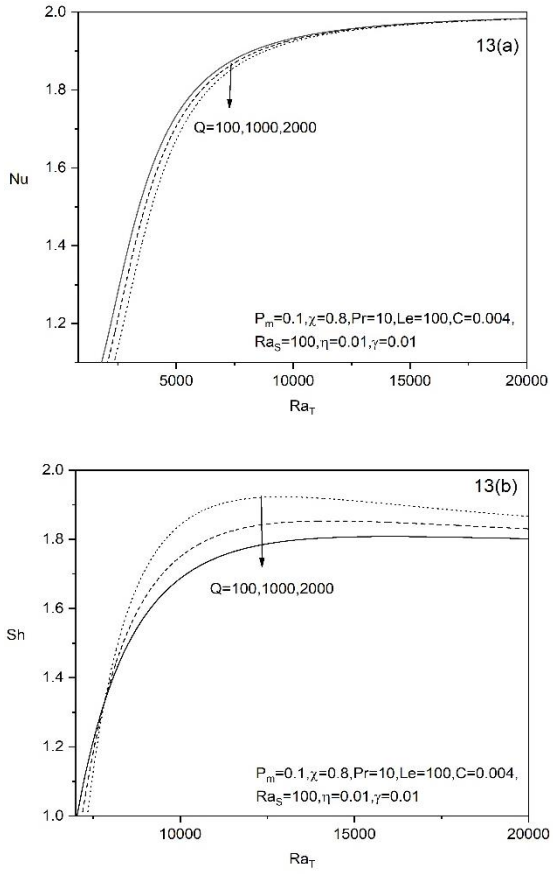

Fig. 13. Variation of Nusselt number and Sherwood number with Ra_T for different values of 13(a) Chandrashekhar number (Q) in (Ra_T ,Nu) plane; 13(b) Chandrashekhar number(Q) in (Ra_T , Sh) plane.

It is discovered from Figures. 14(a)-(b) that the heat and mass transfers in the (Ra_T , Nu) and (Ra_T, Sh) planes decrease as Couple stress parameter C increases. Convection is therefore delayed. This result is similar to the findings of [11]. The physical reason for the delay in the onset of convection is due to the faster heat and mass transfer that occurs when C increases.

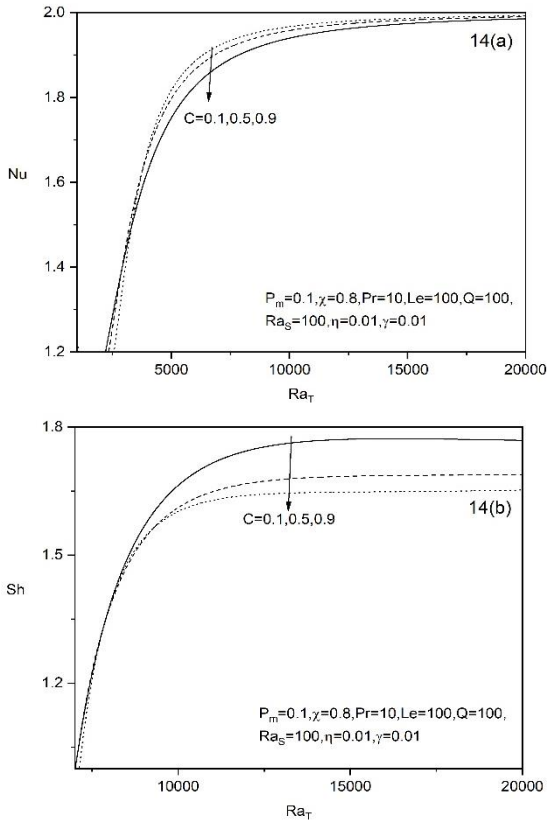

Fig. 14. Variation of Nusselt number and Sherwood number with Ra_T for different values of 14(a) Couple stress parameter (C) in (Ra_T, Nu) plane; 14(b) Couple stress parameter (C) in (Ra_T, Sh) plane.

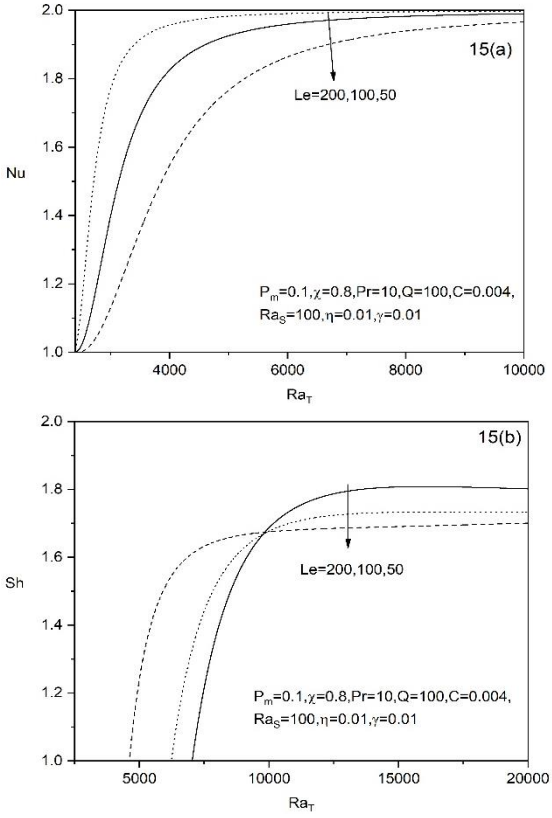

Fig. 15. Variation of Nusselt number and Sherwood number with Ra_T for different values of 15(a) Lewis number (Le) in (Ra_T, Nu) plane; 15(b) Lewis number (Le) in (Ra_T, Sh) plane.

Graphs for various values of the Lewis number (Le) in (Ra_T, Nu) and (Ra_T, Sh) planes are shown in Figures. 15(a)-(b). The graph makes it very evident that Nusselt and Sherwood numbers rise together with an increase in the value of the Le. Convection has improved as a result.

Figures. 16(a)-(b) show graphs for various values of the solutal Rayleigh number (Ra_S). The graph clearly shows that the Nusselt and Sherwood numbers increase as Ra_S increases. Thus, there is advancement in convection.

Although the presence of a stabilising solute gradient will prevent the onset of convection, strong finite amplitude motions that exist for large Rayleigh numbers tend to mix the solute and redistribute it, making the internal layers of the fluid more neutrally stratified. As a result, the inhibitory impact of the solute gradient is significantly diminished, and fluid will convect more and more heat and mass as Ra_S is raised.

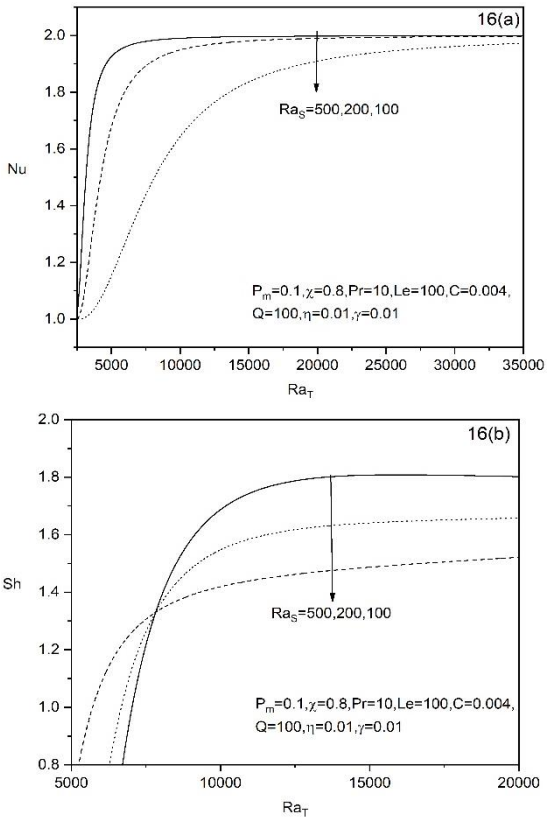

Fig. 16. Variation of Nusselt number and Sherwood number with Ra_T for different values of 16(a) solutal Rayleigh number (Ra_S) in (Ra_T , Nu) plane; 16(b) solutal Rayleigh number (Ra_S) in (Ra_T , Sh) plane.

5.2.2. Unsteady Case (for F/F Boundaries)

For unsteady cases across various short durations (time(t)= 0.01, 0.03, 0.009, 0.006), the patterns of streamlines, isotherms, isohalines, and magnetic streamlines are illustrated in Figures. 17–20.

The streamline pattern is shown in Figures. 17 (a)-(d) for various times. It is shown from the figure that how the streamlines have fewer contours for a short period of time before developing as time passes. The spread of streamlines with time also shows an improvement in convection. It also predicts that as time increases, the magnitude of velocity decreases.

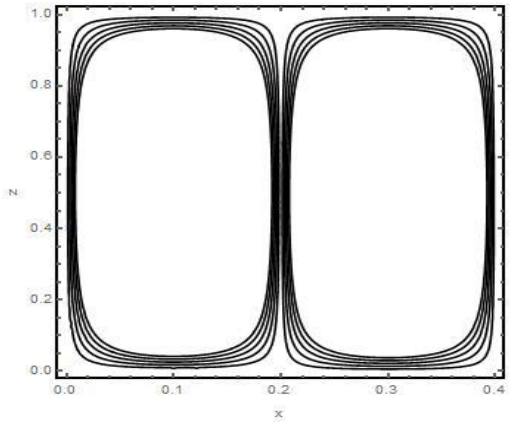

(a)

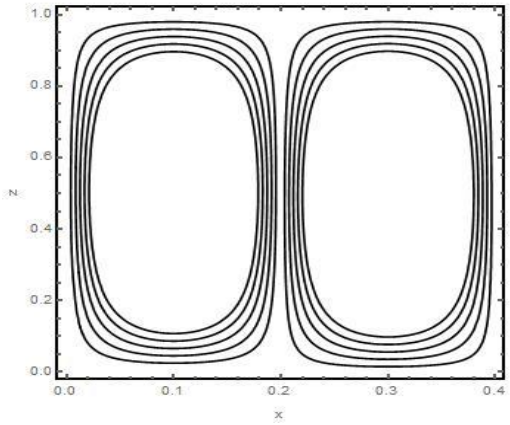

(b)

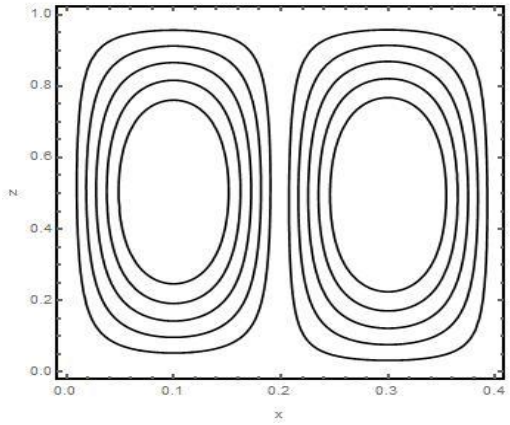

(c)

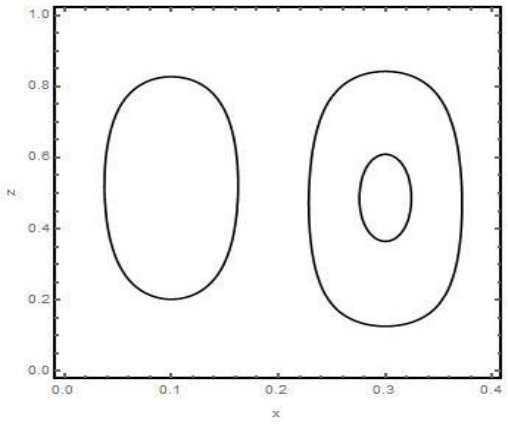

(d)

Fig. 17. Unsteady streamlines for different small time (a) t = 0.01, (b) t = 0.03, (c) t = 0.009, (d) t = 0.006.

The isotherms are shown in Figures. 18 (a)-(d) for various times. These figures make it quite evident that, as time goes on, the convection state manifests itself as a contour.

Heat is observed to be transmitted through conduction at first, but as time goes on, it switches to convection.

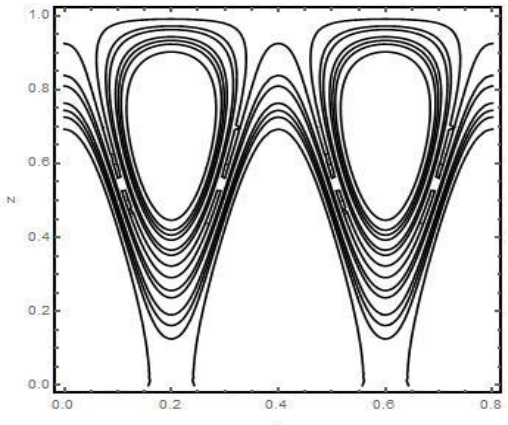

(a)

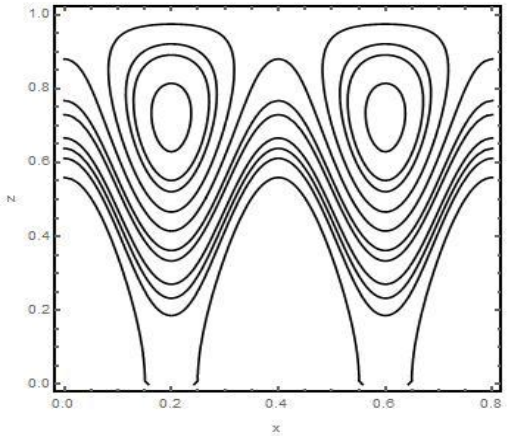

(b)

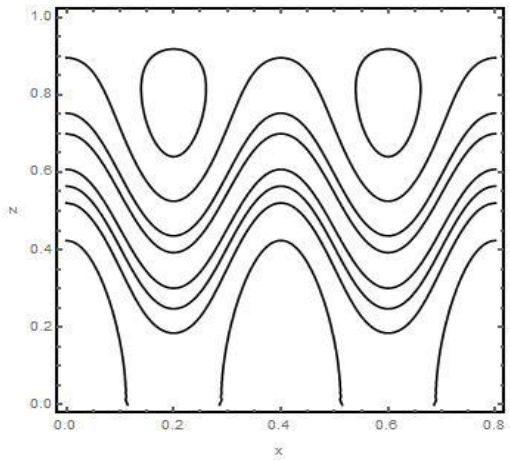

(c)

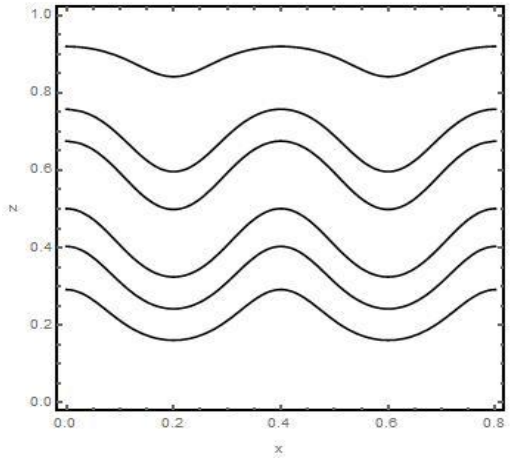

(d)

Fig. 18. Unsteady isotherms for different small time (a) t = 0.01, (b) t = 0.03, (c) t = 0.009, (d) t = 0.006.

Figures. 19 (a)–(d) display the isohalines for various time periods. These figures exhibit isothermal behaviour. These graphs clearly demonstrate how the convection state changes over time as a contour.

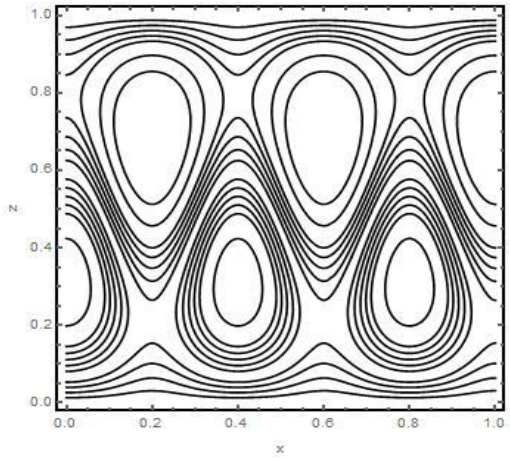

(a)

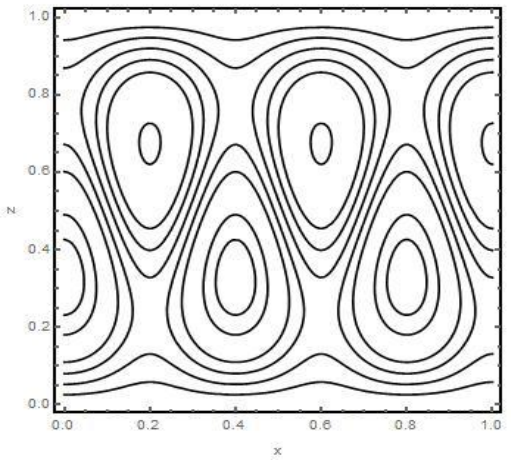

(b)

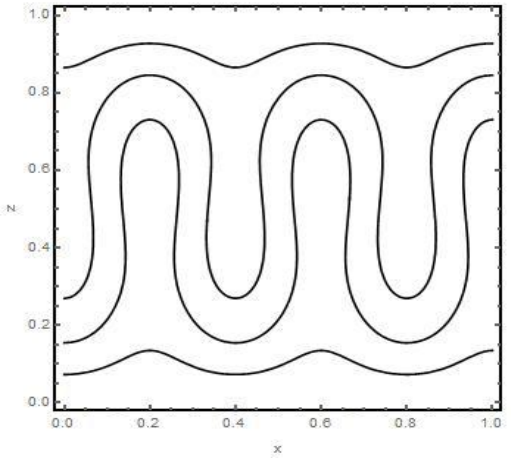

(c)

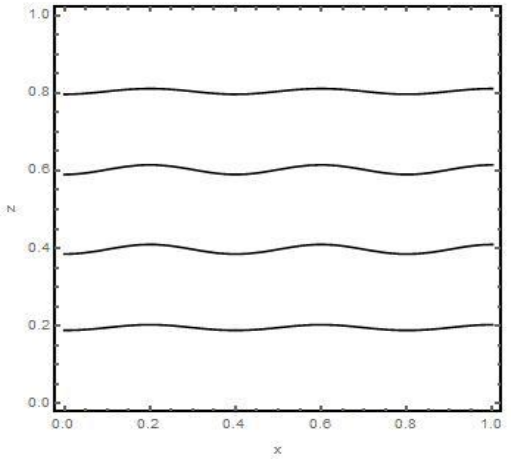

(d)

Fig. 19. Unsteady isohalines for different small time (a) t = 0.01, (b)t = 0.03, (c) t = 0.009, (d) t = 0.006.

The magnetic streamlines for unsteady case are displayed at various time interval in Figures. 20 (a)-(d).

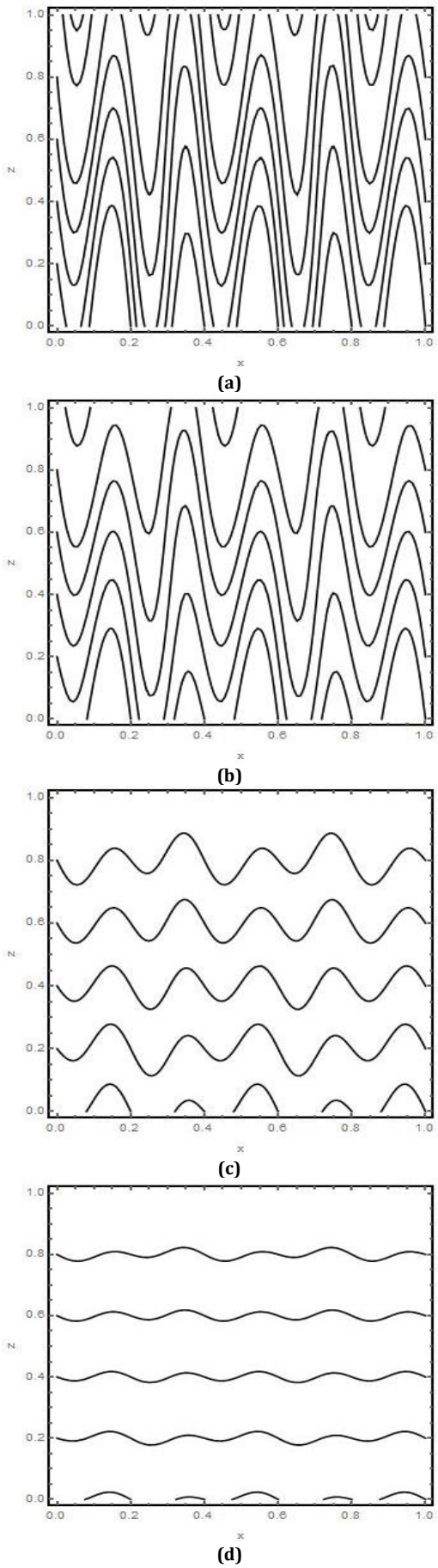

Fig. 20. Unsteady magnetic streamlines for different small time (a) t = 0.01, (b) t = 0.03, (c) t = 0.009, (d) t = 0.006.

6. Conclusions

We have made an effort to comprehend how chemical reactions and magnetic field may affect the onset of thermosolutal convection saturated with couple-stress liquid. Using linear and weakly non-linear stability theories, we examined the impact of different controlling parameters Q, C, χ, Le, χ, Ra_S and γ on the stability of the system. These are our findings.

A comparative study based on boundary surfaces is provided using linear stability theory. The analysis has been performed for four different types of velocity boundary conditions, namely R/R, R/F, F/R,and F/F. For the R/R , F/R and R/F boundaries, the eigenvalue problem is solved using the Galerkin method, whereas exact solutions are obtained for the F/F boundaries. We compared the results among four boundary conditions in the stationary case.

Stability of the system increases with an increase in the values of Chandrashekhar number (Q), Couple stress parameter (C), thermal anisotropic parameter (η) and Lewis number (Le), whereas it decreases with increasing values of Damköhler number (χ). Additionally, the stability criteria for Q came out as (in decreasing order) F/F>F/R>R/R>R/F, which is different from the criteria for the rest of the controlling parameters, i.e F/R>R/R>F/F>R/F. We find that the effect of the solutal Rayleigh number is different for both stationary as well as oscillatory convection for F/F boundaries. For the stationary case, it increases the stability of the system, whereas for the oscillatory case, the stability of the system decreases with an increase in the value of Ra_S when the value of other parameters is fixed. It is found that the Chandrashekhar number (Q), Couple stress parameter (C) and interphase heat transfer coefficient (γ) is responsible for the delay of onset of convection for the oscillatory case and minimum of the critical Rayleigh number shift towards the larger values of the wave number with increasing these parameters. The critical Rayleigh number for the oscillatory case is found to decrease with an increase in the values of χ.

Heat and mass transfer phenomena are observed by non-linear stability analysis using the truncated representation of the Fourier series method. In the steady state, heat and mass transfer decrease with increasing values of the Chandrashekhar number (Q), Couple stress pararmeter (C), thus delaying the onset of convection. Here, heat and mass transfer are measured by the Nussselt and Sherwood numbers, respectively. Nusselt and Sherwood numbers rise along with increases in the value of Lewis number (Le), and solutal Rayleigh number (Ra_S) and amplify the stability of the system. Additionally, over a long period of time, the

Nusselt number and the Sherwood number approach their steady state values. For the unsteady case of non-linear stability analysis, we have discussed streamlines, isotherms, isohalines and magnetic streamlines for different intervals of time.

There has been limited research done on couple stress liquid (in the absence of a body couple) with an externally implied Magnetic or Electric Field. So in the future, it is possible to research magneto-convection or electro-convection on a couple stress liquid with various effects, such as rotation, radiation, LTNE temperature conditions, modulations in various forces, etc.

Nomenclature

a	Wave number [m^{-1}]
a_c	Critical wave number [m^{-1}]
C	Couple stress parameter
d	Height of the fluid layer [m]
g	Acceleration due to gravity [m/s^2]
$\mathcal{H}$	Magnetic field
k	Permeability
Le	Lewis number
Nu	Nusselt number
P	Pressure [kg $m^{-1}s^{-2}$]
Pr	Prandtl number
Pm	Magnetic prandtl number
Q	Chandrashekhar number
Ra_T	Rayleigh number
Ra_S	Solutal Rayleigh number
$\mathcal{C}$	Solute concentration
Sh	Sherwood number
T	Temperature [kelvin]
t	Time [s]
V	Velocity [ms^{-1}]
x,y,z	Space co-ordinates
Greek symbol	
β_T	Coefficient of thermal expansion
β_C	Coefficient of solute expansion
χ	domkohler number
γ	Ratio of heat capacities
κ_T	Thermal diffusivity
κ_C	Solutal diffusivity
μ	Dynamic viscocity
μ_1	Couple stress viscocity
μ_m	Magnetic permeability
σ	Growth rate
ρ	Fluid density [kg m^{-3}]
Λ	Magnetic viscosity

Acknowledgements

Author Monal Bharty gratefully acknowledges the financial assistance from the Central University of Jharkhand as a research fellowship.

Conflicts of Interest

The author declares that there is no conflict of interest regarding the publication of this article. In addition, the authors have entirely observed the ethical issues, including plagiarism, informed consent, misconduct, data fabrication and/or falsification, double publication and/or submission, and redundancy.

Appendix

$$M_1 = \frac{\alpha\alpha_1}{Pra^2} + \frac{\gamma a^2(1+C\alpha)}{\alpha^2},$$

$$M_2 = QP_m^2\pi^2 2^2, \quad M_3 = \alpha^2 P_m^2,$$

$$M_4 = QP_m\pi^2\alpha, \quad M_5 = \frac{\alpha^2\alpha_1(1+C\alpha)}{\alpha^2}$$

$$M_6 = \frac{\gamma\alpha}{Pra^2},$$

$$M_7 = Ra_S\big(\gamma(\alpha_2 + \chi) - (\alpha_1 + \chi)\big),$$

$$M_8 = (\alpha^2 + \chi)^2,$$

$$M_9 = Ra_S(\alpha_1 + \chi)(\alpha_2 + \chi),$$

$$M_{10} = \gamma Ra_S,$$

$$\Pi_2 = M_1\left[1 + \frac{M_2}{M_3+\omega^2}\right] - (M_5 - M_6\omega^2)\left[\frac{M_4}{M_3+\omega^2}\right] + \frac{M_7}{M_8+\omega^2},$$

$$m_1 = P_2 + CP_3, \quad m_2 = \pi a Ra_T$$

$$m_3 = \pi a Ra_S, \quad m_4 = QP_mP_4, \quad m_5 = \pi a$$

$$m_6 = \eta P_1, \quad m_7 = 2\pi^2 a, \quad m_8 = 4\pi^2$$

$$m_9 = \frac{\pi^2 a}{2}, \quad m_{10} = \chi, \quad m_{11} = 2\pi^2 a$$

$$m_{12} = \frac{\pi^2 a^2 + \pi^2}{Le} + \chi, \quad m_{13} = \pi a,$$

$$m_{14} = \frac{4\pi^2}{Le} + \chi, \quad m_{15} = \frac{\pi^2 a}{2}, \quad m_{16} = P_mP_1$$

$$m_{17} = \pi^2 a, \quad m_{18} = \pi, \quad m_{19} = 4P_m\pi^2 a^2$$

$$p_1 = m_2m_5, \quad p_2 = \frac{m_7m_9}{m_8}, \quad p_3 = m_3m_{10},$$

$$p_4 = \frac{m_{13}m_{15}}{m_{14}}, \quad p_5 = m_3m_5m_9m_{12}m_{13}$$

$$p_6 = m_8m_{14}, \quad p_7 = m_4m_{18}, \quad p_8 = \frac{m_{17}m_{20}}{m_{19}}$$

$$p_9 = m_3m_5m_{12}$$

References

[1] Stokes, V.K., 1966. Couple stresses in fluids. Physics of Fluids, 9, pp.1709-1715.

[2] Lin, J.R. and Hung, C.R., 2007. Combined effects of non-Newtonian couple stresses and fluid inertia on the squeeze film characteristics between a long cylinder and an infinite plate. Fluid Dynamics Research, 39, pp.616-631.

[3] Shehawey, E.F.E. and Mekheimer, K.S., 1994. Couple-stresses in peristaltic transport of fluids. Journal of Physics D: Applied Physics, 27, p.1163.

[4] Bodenschatz, E., Pesch, W. and Ahlers, G., 2000. Recent developments in Rayleigh-Bernard convection. Annual Review of Fluid Mechanics, 32, pp.709-778.

[5] Siddheshwar, P.G. and Pranesh, S., 2004. An analytical study of linear and nonlinear convection in Boussinesq–Stokes suspensions. International Journal of Non-Linear Mechanics, 39, pp.165–172.

[6] Sharma, R.C. and Sharma, M., 2004. Effect of suspended particles on couple-stress fluid heated from below in the presence of rotation and magnetic field. Indian Journal of Pure and Applied Mathematics, 35(8), pp.973-989.

[7] Malashetty, M.S. and Basavaraja, D., 2005. Effect of thermal/gravity modulation on the onset of Rayleigh–Benard convection in a couple stress fluid. International Journal of Transport Phenomena, 7, pp.31-44.

[8] Olubode, K., John, O. and Lare, A., 2016. Effects of Some Thermo-Physical Parameters on Free Convective Heat and Mass Transfer over Vertical Stretching Surface at Absolute Zero. Journal of Heat and Mass Transfer Research, 3(1), pp.31-46. doi: 10.22075/jhmtr.2016.424.

[9] Mirzaee, H., Ahmadi, G., Rafee, R. and Talebi, F., 2023. Physical Overview of the Instability in Laminar Wall-Bounded Flows of Viscoplastic and Viscoelastic Fluids at Subcritical Reynolds Numbers. Journal of Heat and Mass Transfer Research, 10(1), pp. 135-146. doi:10.22075/jhmtr.2023.31061.1455.

[10] Umravathi, J.C., Chamkha, A. J., Manjula, M.H. and Al-Mudhaf, A., 2005. Flow and heat transfer of a couple stress fluid sandwiched between viscous fluid layers. Canadian Journal of Physics, 83, pp. 705-720.

[11] Malashetty, M.S., Gaikwad, S.N. and Swamy, M., 2006. An analytical study of linear and non-linear double diffusive convection with soret effect in couple stress liquids. International Journal of Thermal Sciences, 45, pp.897-907.

[12] Gupta, V.K., Singh, A.K., Bhadauria, B.S., Hasim, I. and Jawdat, J.M., 2016. Chaotic convection in couple stress liquid saturated porous layer. International Journal of Industrial Mathematics, 8(2), pp.147-156.

[13] Kiyani, M.Z., Waqas, M., Muhammad, T., Abbasi, A.K., Mamat, M. and Sadiq, M., 2022. Thermally radiative couple-stress magnetized liquid featuring Newtonian heating. Waves in Random and Complex Media. doi: 10.1080/17455030.2022.2044540.

[14] Mishra, P., Reddy, Y.D., Goud, B.S., Kumar, D., Kumar, J. and Singh, P.K., 2022. Study on linear and nonlinear stability analysis of double diffusive electro-convection in couple stress anisotropic fluid-saturated rotating porous layer. Journal of Indian Chemical Society, 99(9), p. 100611.

[15] Pan, Z., Jia, L., Mao, Y. and Wang, Q., 2022. Transitions and bifurcations in couple stress fluid saturated porous media using a thermal non-equilibrium model. Applied Mathematics and Computation, 415, p.126727.

[16] Yadav, D., Mahabaleshwar, U.S., Wakif, A. and Chand, R., 2021. Significance of the inconstant viscosity and internal heat generation on the occurrence of Darcy-Brinkman convective motion in a couple-stress fluid saturated porous medium: an analytical solution. International Communications in Heat and Mass Transfer, 122, p.105165.

[17] Walicki, E. and Walicka, A., 1999. Inertia effects in the squeeze film of a couple-stress fluid in biological bearing. Applied Mechanics and Engineering, 4, pp.363–373.

[18] Kaufman, J., 1994. Numerical models of fluid flow in carbonate platforms: implications for dolomitization. Journal of Sedimentary Research A, 64, pp.128-139.

[19] Gilman, A. and Bear, J., 1994. The influence of free convection on soil salinization in arid regions. Transport in Porous Media, 23, pp.275-301.

[20] Wit, A.D., 2001. Fingering of Chemical Fronts in Porous Media. Physics Review Letter, 87, p. 054502.

[21] Wit, A.D., 2004. Miscible density fingering of chemical fronts in porous media: nonlinear simulations. Physics of Fluids, 16, pp.163-175.

[22] Srivastava, A. K. and Bera, P., 2013. Influence of Chemical reaction on the stability of Thermo-Solutal convection of

couple stress fluid in a Horizontal porous layer. Transport in porous Media, 97, pp. 161-184.

[23] Aly, A., Chamkha, A.J. and Raizah, Z.A.S., 2020. Radiation and Chemical Reaction Effects on Unsteady Coupled Heat and Mass Transfer by Free Convection from a Vertical Plate Embedded in Porous Media. Journal of Heat and Mass Transfer Research, 7(2), pp. 95-103. doi: 10.22075/jhmtr.2019.10763.1149.

[24] Ramachandramurthy, V., Kavitha, N. and Aruna, A.S., 2022. The effect of a magnetic field on the onset of Bénard convection in variable viscosity couple-stress fluids using classical Lorenz model. Applications of Mathematics, 67, pp.509–523 .

[25] Bormudoi, M. and Ahmed, N., 2023. Convective MHD flow of a rotating fluid past through a moving isothermal plate under diffusion-thermo and radiation absorption. Journal of Heat and Mass Transfer Research, doi: 10.22075/jhmtr.2023.31013.1454.

[26] Saravana, R., Sreenadh, S., Venkataramana, S., Reddy, R.H. and Kavitha, A., 2011. Influence of slip conditions, wall properties and heat transfer on MHD peristaltic transport of a Jeffery fluid in a non-uniform porous channel. International Journal of Inovative Technology and Creative Engineering, 11(1), pp.10-24.

[27] Parker, E.N., 1966. The dynamical state of the interstellar gas and field. The Astrophysical Journal, 145, pp.811–833.

[28] Stella, L. and Rosner, R., 1984. Magnetic field instabilities in accretion disks. The Astrophysical Journal, 277, pp.312–321.

[29] Hughes, D.W., 2007. Magnetic buoyancy instabilities in the tachocline. In The Solar Tachocline. Cambridge University Press, pp.275-298.

[30] Narahari, M. and Debnath, L., 2013. Unsteady magnetohydrodynamic free convection flow past an accelerated vertical plate with constant heat flux and heat generation or absorption. Journal of Applied Mathematics and Mechanics, 93(1), pp.38–49.

[31] Srivastava, A. K., Bhadauria, B. S. and Gupta, V. K., 2012. Magneto-convection in an anisotropic porous layer with Soret effect. International Journal of non-linear Mechanics, 47, pp.426-438.

[32] Siddique, I. and Mirza, I.A., 2016. Magneto-hydrodynamic free convection flows of a viscoelastic fluid in porous medium with variable permeability heat source and chemical reaction. Results in Physics, 7, pp.3928-3937.

[33] Wilczynski, F., Hughes, D.W. and Kersale, E., 2022. Magnetic buoyancy instability and the anelastic approximation: regime of validity and relationship with compressible and Boussinesq descriptions. Journal of Fluid Mechanics, 942, A46, pp.1-38. doi:10.1017/jfm.2022.325.

[34] Meenakshi, V., 2014. Dufour and Soret Effect on Unsteady MHD Free Convection and Mass Transfer Flow Past an Impulsively Started Vertical Porous Plate Considering with Heat Generation. Journal of Heat and Mass Transfer Research, 8, pp.257-266.

[35] Mohammad, N., Mohammad, S. and Ahmad, R.R., 2021. Analysis of the Effect of Periodic Magnetic Field, Heat Absorption/Generation and Aspect Ratio of the Enclosure on Non-Newtonian Natural Convection. Journal of Heat and Mass Transfer Research, 8, pp.187-203.

[36] Sahay, J.A., Saikrishnan, P., and Natarajan, E., 2022. Unsteady Magnetohydrodynamic Mixed Convection Flow over a Rotating Sphere with Sinusoidal Mass Transfer, Journal of Heat and Mass Transfer Research, 9, pp.129-140.

[37] Siddabasappa, C., Siddheshwar, P.G. and Makinde, O.D., 2021. A study on entropy generation and heat transfer in a magnetohydrodynamic flow of a couple-stress fluid through a thermal nonequilibrium vertical porous channel. Heat Transfer, pp.1-24.

[38] Mahesh, R., Mahabaleshwar, U.S., Kumar, P.N.V., Öztop, H.F. and Hamdeh, N.A., 2023. Impact of radiation on the MHD couple stress hybrid nanofluid flow over a porous sheet with viscous dissipation. Results in Engineering, 17, p.100905.

[39] Phillips, O. M., 2009. Geological Fluid Dynamics. Cambridge University Press, New York.

[40] Chandrasekhar, S., 1981. Hydrodynamic and Hydromagnetic Stability. Dover: New York.

[41] Finlayson, B.A., 2006. The Method of Weighted Residuals and Variational Principals. Academic Press: London.

[42] Pritchard, D. and Richardson, C.N., 2007. The effect of temperature-dependent solubility on the onset of thermosolutal convection in a horizontal porous layer. Journal of Fluid Mechanics, 571, pp.59–95.